WL-TR-91-4137

COMPUTER SIMULATION OF CYCLIC SILOXANE-BASED LIQUID CRYSTALS: MOLECULAR DYNAMICS AND X-RAY SCATTERING

E. P. Socci and B. L. Farmer
Department of Materials Science
University of Virginia
Charlottesville, Virginia 22901

R. Pachter and W. W. Adams
WL/MLPJ, Wright Laboratory, Materials Directorate
Wright-Patterson Air Force Base, Ohio 45433-6533

T. J. Bunning
Department of Chemical Engineering
University of Connecticut
Storrs, Connecticut 0626

January 1992

Final Report for the Period May 1991 - August 1991

Approved for public release; distribution is unlimited

MATERIALS DIRECTORATE
WRIGHT LABORATORY
AIR FORCE SYSTEMS COMMAND
WRIGHT-PATTERSON AIR FORCE BASE OHIO 45433-6533

NOTICE

WHEN GOVERNMENT DRAWINGS, SPECIFICATIONS, OR OTHER DATA ARE USED FOR ANY PURPOSE OTHER THAN IN CONNECTION WITH A DEFINITELY GOVERNMENT-RELATED PROCUREMENT, THE UNITED STATES GOVERNMENT INCURS NO RESPONSIBILITY OR ANY OBLIGATION WHATSOEVER. THE FACT THAT THE GOVERNMENT MAY HAVE FORMULATED OR IN ANY WAS SUPPLIED THE SAID DRAWINGS, SPECIFICATIONS, OR OTHER DATA, IS NOT TO BE REGARDED BY IMPLICATION, OR OTHERWISE IN ANY MANNER CONSTRUED, AS LICENSING THE HOLDER, OR ANY OTHER PERSON OR CORPORATION; OR AS CONVEYING ANY RIGHTS OR PERMISSION TO MANUFACTURE, USE, OR SELL ANY PATENTED INVENTION THAT MAY IN ANY WAY BE RELATED THERETO.

THIS REPORT HAS BEEN REVIEWED BY THE OFFICE OF PUBLIC AFFAIRS (ASD/PA) AND IS RELEASABLE TO THE NATIONAL TECHNICAL INFORMATION SERVICE (NTIS). AT NTIS, IT WILL BE AVAILABLE TO THE GENERAL PUBLIC INCLUDING FOREIGN NATIONALS.

THIS TECHNICAL REPORT HAS BEEN REVIEWED AND IS APPROVED FOR PUBLICATION.

R L Crane

ROBERT. L. CRANE, Project Scientist
Hardened Materials Branch
Electromagnetic Mat'ls & Surv Div

Gary K. Waggoner

GARY K. WAGGONER, Chief
Hardened Materials Branch
Electromagnetic Mat'ls & Surv Div

William R Woody

WILLIAM R. WOODY, Chief
Electromagnetic Mat'ls & Surv Div

If your address has changed, if you wish to be removed from out mailing list, or if the addressee is no longer employed by your organization, please notify WL/MLPJ, Wright-Patterson AFB OH 45433-6533 to help us maintain a current mailing list.

Copies of this report should not be returned unless return is required by security considerations, contractual obligations, or notice on a specific document.

REPORT DOCUMENTATION PAGE

Form Approved
OMB No 0704-0188

1 AGENCY USE ONLY (Leave blank)	2 REPORT DATE	3 REPORT TYPE AND DATES COVERED
	JANUARY 27,1992	Final: MAY 91 - AUG 91

4 TITLE AND SUBTITLE
COMPUTER SUMULATION OF CYCLIC SILOXANE - BASED LIQUID CRYSTALS: MOLECULAR DYNAMICS AND X-RAY SCATTERING

5. FUNDING NUMBERS
PE - 62102F
PR - 2422
TA - 04
WU - 01

6 AUTHOR(S)
E.P. SOCCI; B. L. FARMER; R. PACHTER; W.W. ADAMS; T. BUNNING

7 PERFORMING ORGANIZATION NAME(S) AND ADDRESS(ES)
Wright Laboratory, Materials Directorate
WL/MLPJ
Wright-Patterson Air Force Base
Ohio 45433-6533

8 PERFORMING ORGANIZATION REPORT NUMBER
WL-TR-91-4137

9 SPONSORING/MONITORING AGENCY NAME(S) AND ADDRESS(ES)

10 SPONSORING/MONITORING AGENCY REPORT NUMBER

11. SUPPLEMENTARY NOTES

12a DISTRIBUTION/AVAILABILITY STATEMENT
Approved for public release; distribution unlimited.

12b. DISTRIBUTION CODE

13 ABSTRACT *(Maximum 200 words)*

The molecular dynamics technique is employed in the present study to investigate molecular models of a liquid crystal (LC) based on cyclic penta(methylsiloxane) with combinations of cholesteryl-4'-allyloxybenzoate and biphenyl-4'allyloxybenzoate mesogens, which is of technological importance because of attributes related to light processing media The packing and structure exhibited by these commercially available cholesteric LC's show unusually well-defined interlayer order giving rise to high order X-ray reflections The purpose of this investigation was to. (1) Investigate the conformational flexibility of the molecular arrangements and organization of this cyclic siloxane-based LC at room temperature, providing insight into the relative stability of the various models proposed (2) Serve as an instructional reference describing the basic theory and use of molecular mechanics and dynamics for the study of large molecular systems Results from the molecular dynamics calculations indicate the degree of conformational flexibility among the pendant mesogens of this molecular system, and its effects on interdigitation I. particular, the isolated disk model exhibits the most flexibility and greatest stability as indicated by mean dihedral angles and range for certain key torsions. The dynamics simulation of the cylinder pairs suggests a large conformational flexibility of the siloxane rings. Also, movements of the interdigitated mesogens were much higher for a fixed rings system than for the case where the ring atoms were free to move X-ray scattering pattern calculations for the structures generated during the dynamics run demonstrate higher order than for the initial models

14 SUBJECT TERMS	15 NUMBER OF PAGES
SILOXANES; X-RAY SCATTERING; COMPUTATINAL CHEMISTRY; MOLECULAR MECHANICS/DYNAMICS; LIQUID CRYSTALS; MOLECULAR MODELING	58
	16 PRICE CODE

17 SECURITY CLASSIFICATION OF REPORT	18 SECURITY CLASSIFICATION OF THIS PAGE	19 SECURITY CLASSIFICATION OF ABSTRACT	20 LIMITATION OF ABSTRACT
UNCLASSIFIED	UNCLASSIFIED	UNCLASSIFIED	UNLIMITED

FOREWORD

This report was prepared by the Laser Hardened Materials Branch, Electromagnetic Materials and Suvivability Division. The work was initiated under Project No 2422, "Laser Hardened Materials." It was administered under the direction of the Materials Directorate, Wright Laboratory, Air Force Systems Command, Wright-Patterson Air Force Base, Ohio, with Dr R. L. Crane as the Materials Laboratory Project Scientist (WUD26 Leader). The authors were Drs W. Wade Adams and Ruth Pachter, WL/MLPJ, Wright Laboratory, Materials Directorate, Wright-Patterson Air Force Base, Ohio 45433-6533, E. P. Socci and Dr B. L. Farmer, Department of Materials Science, University of Virginia, Charlottesville, Virginia 22901, and T. J. Bunning, Department of Chemical Engineering, University of Connecticut.

We thank the Polymer Branch, Materials Directorate, Wright Laboratory, for their generosity in the use of the Quanta/CHARMm program on their Silicon Graphics system. We are especially grateful for the computer support provided by Mr. Jacque Henes, Polymer Branch, Materials Directorate, Wright Laboratory.

TABLE OF CONTENTS

LIST OF TABLES

Section 1

INTRODUCTION

Side-chain thermotropic liquid crystalline (LC) materials have been investigated for possible applications in electro-optical devices[1], nonlinear optics[2,3], selective optical filters and reflectors[4,5], and optical storage media[6,7]. In particular, linear polysiloxane polymers have received considerable attention, as a promising backbone moiety due to their low glass transition temperatures. The flexibility of this backbone minimizes the dynamic coupling of the main- and side-chain motions. Recently, several groups have also reported on possible microphase separation of the hydrocarbon side-chain mesogens from the linear siloxane backbone based on experimental X-ray diffraction results[8-10]. Electron density calculations[8] indicate that the smectic layer can be divided into sublayers which consist of a mesogenic core, spacer groups, and aliphatic tails with the siloxane backbone forming a thin (5 Å-7 Å) interface between layers.

Liquid crystalline systems of increasing interest consist of small siloxane rings with different pendant mesogenic groups attached, for example, a mixed cyanoester and cyanobiphenyl system[11]. Another such LC is based on cyclic penta(methylsiloxane) with combinations of cholesteryl-4'-allyloxybenzoate {C} (40% mole fraction) and biphenyl-4'allyloxybenzoate {B} (60% mole fraction) mesogens (cf. Figure 1). The packing and structure exhibited by these commercially available cholesteric LC's (Wacker LC-Silicones)[12] have been recently studied, showing unusually well-defined interlayer order giving rise to high order X-ray reflections[13]. This LC is of technological importance because of attributes related to light processing media[5,6].

Molecular mechanics and dynamics are well established techniques for macromolecular structural definition[14] at the atomic level, applied, for example, for polymeric chains[15a,b]. A molecular simulation of a cyclic siloxane-based liquid crystal model by employing semiempirical and molecular mechanics calculations was recently performed[16]. This computational study offered an insight into the effects of molecular structure on the intramolecular interactions and also the

THIS
PAGE
IS
MISSING
IN
ORIGINAL
DOCUMENT

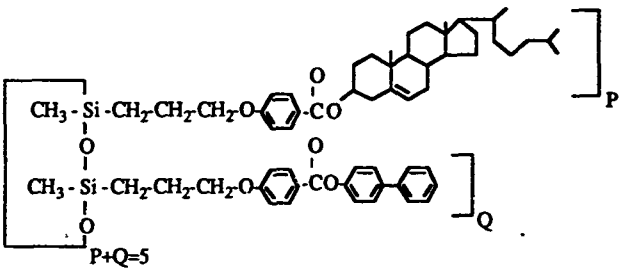

Figure 1: The chemical structure of the studied cyclic siloxane - based liquid crystal.

Section 2

THEORY

2.1. MOLECULAR MODELING

The molecular mechanics and molecular dynamics modeling methods are employed here to study the packing geometries of a cyclic siloxane-based LC. In order to perform a molecular dynamics simulation, one must first describe the potential energy surface of the molecular system in question. The potential energy surface is obtained in this case by the application of the semi-classical molecular mechanics (MM) approach. An MM calculation of a molecule evaluates its conformational energy, and an energy minimization represents it as it would exist near 0° K. By simulating a molecule at elevated temperatures for the calculation of structural fluctuations, phase transitions and time averaged properties, the molecular dynamics application is used to partition the total energy between kinetic and potential contributions, and to distribute the latter between the vibrational states of the molecule. Molecular mechanics and molecular dynamics calculations in this study were performed by using the Quanta/CHARMm[17] molecular modeling computer software on a Silicon Graphics workstation.

2.1.1. Molecular Mechanics

2.1.1.1 Potential Energy

In the molecular mechanics methodology the potential energy of a molecule or group of molecules is expressed in a classical approach as the sum of terms describing the state of the system. These include bond lengths, bond angles, torsion angles and nonbonded pairwise interactions. The potential energy of a system of configuration r may then be written as follows:

$$V(r)=1/2\Sigma K_b(b-b_0)^2+1/2\Sigma K_\theta(\theta-\theta_0)^2+1/2\Sigma K_\varphi(1+\cos(n\varphi-\delta))+\Sigma(A/r^{12}-C/r^6+q1q2/Dr) \quad (1)$$

bonds bond angles torsion angles non-bonded pairs

where b, θ, φ, and r denote bond lengths, bond angles, torsion angles and nonbonded intramolecular distances, respectively. The force field parameters K_b, K_θ, K_φ, A, C, and D, the geometrical values b_0, θ_0, n, δ and the partial atomic charges q are described for the CHARMm[15] force-field in Reference 18. The parametrization for the organosiloxane derivatives are taken from Reference 19, and the partial atomic charges for the siloxane ring from Reference 16.

In order to calculate the potential energy of a molecule, or group of molecules, by the use of equation (1), a set of {x, y, z} cartesian coordinates is required to describe the position r of each atom. For example, the contribution to the potential energy expression from the bond lengths would be calculated as described in the following. First, the bond length b_{ij} between two bonded atoms is calculated:

$$b_{ij} = \{ (x_i - x_j)^2 + (y_i - y_j)^2 + (z_i - z_j)^2 \}^{1/2} \quad (2)$$

where $\{x_i, y_i, z_i\}$, and $\{x_j, y_j, z_j\}$, are the cartesian coordinates for atoms i and j, respectively. The standard (optimum) value for this particular bond length (b_0) is then subtracted from the value determined in equation (2). In order to obtain the potential energy of this bond length, the $(b - b_0)^2$ term is multiplied by an appropriate force constant, K_b. The procedure is repeated for all of the bonds present within the molecule[17]. Such calculations are performed for all energy terms in equation (1). A decrease in computation time of the nonbonded atom pair interactions term is obtained by introducing a cut off distance (8 Å - 15 Å depending upon the molecular size).

2.1.1.2 Energy Minimization

Once the potential energy surface of the molecule is described, its conformation can be varied in an effort to reduce the potential energy of the system and better describe the lowest energy

geometry. Several energy minimization techniques can be invoked for energy minimization. The simplest procedure (and often most usefui) is the Steepest Descent method which involves the calculation of the gradient of the potential energy of the system with respect to the coordinates. Specifically, an iterative process is performed in which the gradient of the potential is calculated with respect to a particular set of coordinates. A new value of the coordinates is then found which lowers the potential energy of the system. A constant (typically 1.2) is then multiplied by the negative gradient of the potential and a new energy calculated. If the energy decreases, the process continues. If the energy increases after a step has been taken, the step size is reduced by a factor (typically 0.5) for the next iteration[20]. Equation (3) describes one iteration (i) of this procedure for the minimization of a torsion angle φ:

$$\varphi^i = \varphi^{i-1} - k\partial V/\partial\varphi \qquad (3)$$

Although the Steepest Descent method is suitable for removing major distortions in geometry or improper steric interactions, it may locate local potential energy minima (rather than a global minimum) for the molecular geometry[21]. Thus, more powerful energy minimization techniques have been developed such as the Conjugate Gradient method and the Newton-Raphson method, discussed extensively elsewhere[21].

2.1.2. Molecular Dynamics

2.1.2.1 General

Molecular dynamics calculations simulate the natural motion of a molecular system and produce a set of trajectories which describe the atomic motions of the system over time[21]. Calculations can be performed at constant temperature or constant pressure. They yield various time averaged properties of the system, such as potential, kinetic or total energies of the system, torsion angles, interatomic distances and bond angles. In addition, the trajectories show the "instantaneous" values of these quantities as a function of time. In general, molecular dynamics

calculations have proved to be useful in examining the behavior of molecular systems over time at specified temperatures or pressures.

2.1.2.2 Methodology

Consider a system of N atoms, where atom i has mass m_i and position $\mathbf{r}_i$. The relationship between the velocity ($d\mathbf{r}_i / dt$) and the momentum ($\mathbf{p}_i$) of the atom is given by:

$$d\mathbf{r}_i / dt = \mathbf{p}_i / m_i \qquad (4)$$

Substituting this into Newton's equation of motion, $\mathbf{F} = m\mathbf{a}$, yields:

$$\mathbf{F}_i = d\mathbf{p}_i / dt \qquad (5)$$

where $\mathbf{F}_i$ is the net force exerted on atom i by all of the other atoms in the system. Since the force is the negative of the gradient of the potential energy, equation (5) can be rewritten as:

$$\mathbf{F}_i = -\partial V / \partial \mathbf{r}_i = d\mathbf{p}_i / dt \qquad (6)$$

The force, $\mathbf{F}_i$ is obtained from the gradient of the potential energy (equation (1)). By integrating equation (6) over small enough time steps ($\Delta t \sim 1/2$ fs), the velocity and position of each atom can be updated to a new velocity and position by using the Verlet numerical integration method[22]. The procedure yields a trajectory for the molecular system over some specified time period.

The molecular dynamics calculation may be performed at constant temperature by making use of the following relationship:

$$3 k_b T = \Sigma m_i v_i \cdot v_i / N \qquad (7)$$

where k_b is the Boltzmann constant. In order to keep the temperature of the system constant, the velocities of the atoms are adjusted appropriately (scaled) using a method developed by Anderson[23].

It is appropriate to note that in most cases, molecular dynamics calculations require a large amount of computer time. In order to reduce computation time the SHAKE algorithm[25] may be employed, which allows the user to increase the time step used in the calculation and thereby reduce the total number of iterations to complete one simulation. The time step used must be small compared to the period of the highest frequency motion of interest in the system. Because C-H stretching is typically the highest frequency of vibration in a molecule, SHAKE is used to fix these bonds at their original equilibrium values. So doing, the time step used in a molecular dynamics simulation can be increased by a factor of 2, i.e.,to a value of 1 femtosecond (fs).

2.1.2.3 Simulation Procedure

A molecular dynamics simulation consists of heating, equilibration and simulation steps, briefly described below.

2.1.2.3.1. Heating

The first step in a molecular dynamics simulation is obtaining a set of cartesian coordinates for the atoms constituting the molecule or group of molecules. From these the potential energy surface is specified by using the MM potential function described in equation (1). In addition, prior to the initiation of a molecular dynamics calculation, the potential energy of the molecular system should be partially minimized to remove major distortions in geometry or improper steric interactions.

This minimized starting structure, with all atoms having zero velocities, represents the molecular system at a temperature near absolute zero. In order to perform a molecular dynamics simulation at a higher temperature, it is necessary to heat the molecule. Heating is generally accomplished by slowly and uniformly adding kinetic energy to the molecular system at periodic time intervals by assigning velocities to each atom, either randomly or in proportion to the force acting on the atom. The length of the heating period is extremely important and is dependent upon the size of the molecular system. If the heating period is too short, achieving a constant temperature may prove to be impossible in the equilibration and simulation stages. For a system containing approximately 700 atoms (such as some of those studied here), a heating time of approximately 2 pico seconds is sufficient. Smaller systems can be heated faster and larger systems should be heated longer.

2.1.2.3.2. Equilibration

After the system is heated to the desired temperature, it is necessary to equilibrate it over a period of time sufficient to make the total energy of the system (potential + kinetic) remain constant. This procedure uses as input the dynamics files created from the heating phase of the simulation. Equilibration is continued until the total energy becomes constant over time.

2.1.2.3.3. Simulation

After the system has been equilibrated at the desired temperature, the simulation phase is carried out for 10 ps or more in order to get reasonable time averaged results and other statistical or thermodynamic information. The simulation step uses as input the dynamics files created during the equilibration phase of the calculation.

2.2. X-RAY DIFFRACTION CALCULATION

Cylindrically averaged scattering is the most common technique for modeling scattering from an anisotropic material, namely oriented with (cylindrical) symmetry, without assuming any crystalline order[26]. Averaging is performed by rotation around the axis of the direction of the fibrous microscopic model (by convention the z axis), so that the intensity transform $I(R, Z)$ is cylindrically symmetrical about it. This simulation is most applicable for highly oriented materials, such as in the LC state[26,27]. The Fourier-integral of the scattering amplitude for n atoms is :

$$F(\mathbf{S}) = \sum_{j}^{n} f_j(s) e^{2\pi i(\mathbf{S}\cdot\mathbf{r}_j)} \qquad (8)$$

where f_j indicates the scattering power, $\mathbf{S}$ the reciprocal lattice vector, and $\mathbf{r}_j$ the interatomic vector in real space. It can be shown that this can be expressed in terms of the n-th order Bessel function J_n for a solution in cylindrical coordinates[26] :

$$I(R,Z) = \sum_{n} \left(\sum_{j} f_j J_n(Rr_j) \cos(Zz_j - n\phi_j)\right)^2 + \sum_{n} \left(\sum_{j} f_j J_n(Rr_j) \sin(Zz_j - n\phi_j)\right)^2 \qquad (9)$$

where $(R, Z, \psi;\ X=R\cos\psi,\ Y=R\sin\psi,\ Z=Z)$ and $(r, z, \phi;\ x=r\cos\phi,\ y=r\sin\phi,\ z=z)$, are the cylindrical coordinates in reciprocal and direct space, respectively, and $I = |F|^2$. Note that I is only a function of R and Z for the cylindrical symmetrical component, being averaged with respect to ψ for the oriented sample. The summation in equation (9) is done for all atoms j, and $-5<n<+5$, since only these terms of the Bessel function are of importance[26,27].

Spurious features which may occur in this general diffraction simulation of molecular models are eliminated by using a model-size correction; in particular, the cylindrically averaged scattering is subtracted from that derived for a prism, or cylinder, with the same radial structure as the model but structureless in the z - direction. Such a calculation describes a special case of the above general formulation in equation (9)[26]. This total scattering, including the model-size correction as well as the meridional section (namely the Fourier transform of the projection of the structure onto the z axis) were calculated by the CERIUS simulation program[27].

Section 3

RESULTS AND DISCUSSION

3.1. Dynamics on Isolated Molecules

An understanding of the conformational flexibility and degree of interdigitation in the cyclic siloxane-based LC shown in Figure 1, may be initially obtained by molecular dynamics calculations on the isolated molecular models. The three models are those in which all mesogens are either axial or equatorial (shown in Figures 2 and 3, respectively), or at an intermediate conformation (shown in Figure 4) in which two {C} sidechains are in the axial position, and three {B} sidechains are in the equatorial position. In these three figures, the sizes of the silicon atoms are not proportional to those of the other atoms. These have been termed the cone, disk and cylinder models[13], respectively, because of their characteristic geometries, and have been previously studied[16]. Details of the molecular dynamics simulations are presented in Table Ia.

Structural differences between the starting models (Figures 2-4) and those from the molecular dynamics calculation (Figures 5-7) were examined. The structures shown in Figures 5-7 are the lowest energy and averaged structures of the simulation after a 10 pico second run at 300° K. Clearly, a comparison of Figures 2-4 and 5-7 shows a great deal of conformational variations. Further analysis was carried out by comparing various torsional angles during the simulation to those in the initial structure.

The mean variation of a torsion angle during the molecular dynamics run is derived from a histogram plot of the dihedral angle distribution during the simulation, from which the mode can be determined. This, in turn, approximates the mean since a normal distribution is generally observed. As an example, Figure 8 shows a histogram for one of the five dihedral angles within a mesogen. Specifically, *Tor1*, the first rotatable bond of the mesogen {O-Si-$C_{\text{first of spacer-mesogen}}$-$C_{\text{second of spacer-mesogen}}$} is plotted. Tables II and III summarize the mean magnitudes and range of

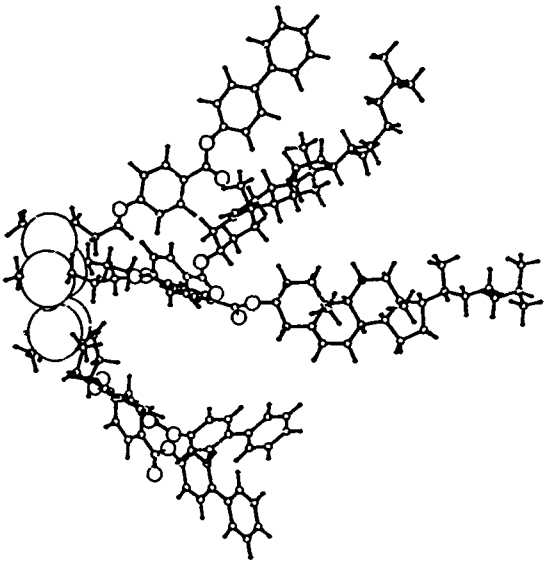

Figure 2: Optimized geometry of the model used in the calculations in which all pendant groups are in axial position.

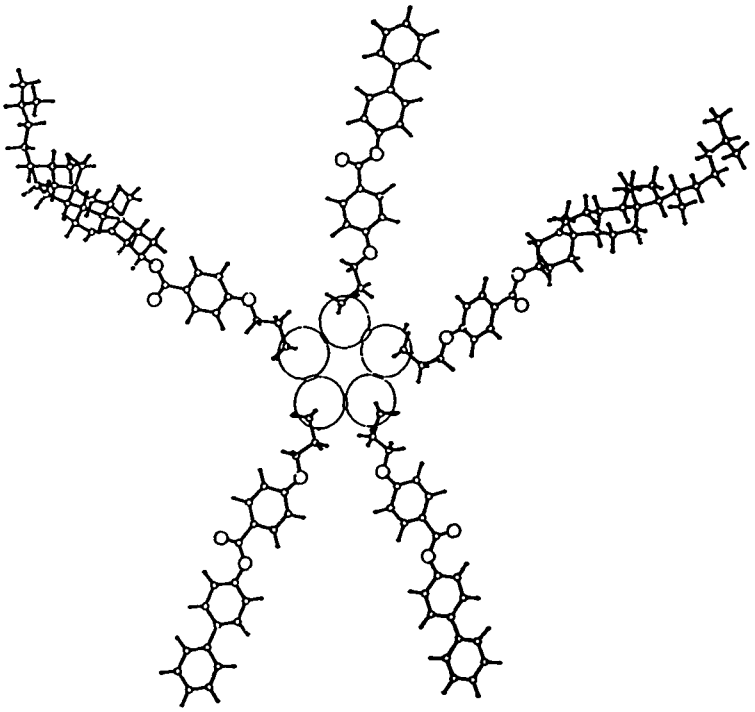

Figure 3: Optimized geometry of the model used in the calculations in which all pendant groups are in the equatorial position.

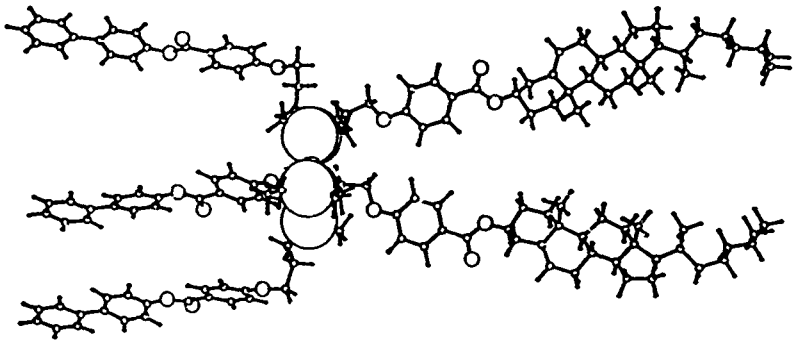

Figure 4: Optimized geometry of the model used in the calculations in which the two cholesteryl groups are axial and the three biphenyl groups are equatorial.

TABLE I : Details of Molecular Dynamics Simulation[a]

(a) Isolated Cone, Disk and Cylinder Models

	Cone[b]	Disk[b]	Cylinder[c]
Heating time (ps)	0.5	0.5	2.5
Equilibration time (ps)	64.0	5.5	41.5
Simulation time(ps)	10.0	10.0	10.0
Time step (ps)	0.0005	0.0005	0.001

(b) Unconstrained Cylinder Molecular Pairs (CASE I)[c]

Heating time (ps)	2.5
Equilibration time (ps)	130.0
Simulation time(ps)	10.0
Time step (ps)	0.0005

(c) Constrained Cylinder Molecular Pairs (CASE II)[c]

Heating time (ps)	5.0
Equilibration time (ps)	40.0
Simulation time(ps)	10.0
Time step (ps)	0.001

(d) Constrained Disk Molecular Pairs (CASE III)[c]

Heating time (ps)	5.0
Equilibration time (ps)	10.0
Simulation time(ps)	10.0
Time step (ps)	0.001

[a] Non bonded cut off distance : 8 Å; nonbonded pair list update frequency : every 50 iterations.
[b] The SHAKE procedure was not applied.
[c] The SHAKE procedure was applied.

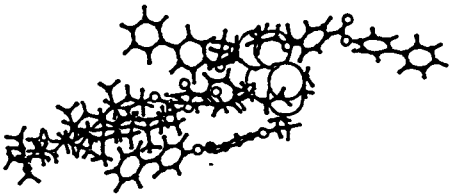

(a)

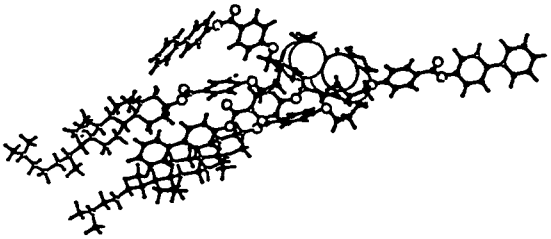

(b)

Figure 5: Model structures of the cone isomer after a 10 pico second molecular dynamics simulation. The upper structure (a) is the lowest energy conformation adopted during the simulation. The lower structure (b) is the statistically averaged structure of the molecule during the 10 pico second simulation.

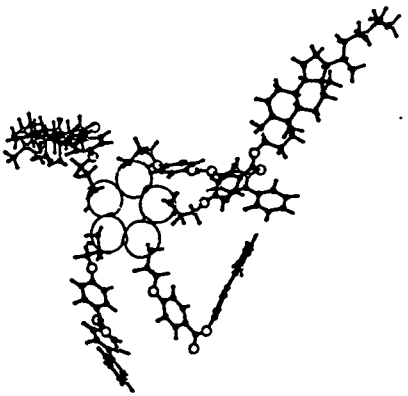

(a)

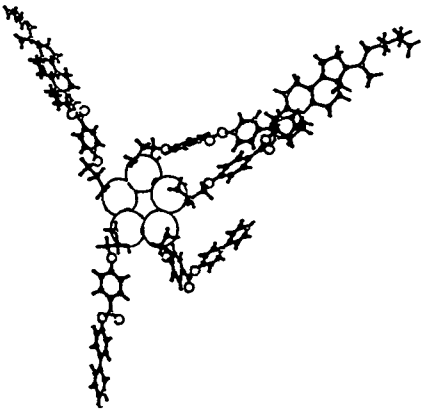

(b)

Figure 6: Model structures of the disk isomer after a 10 pico second molecular dynamics simulation. The upper structure (a) is the lowest energy conformation adopted during the simulation. The lower structure (b) is the statistically averaged structure of the molecule during the 10 pico second simulation.

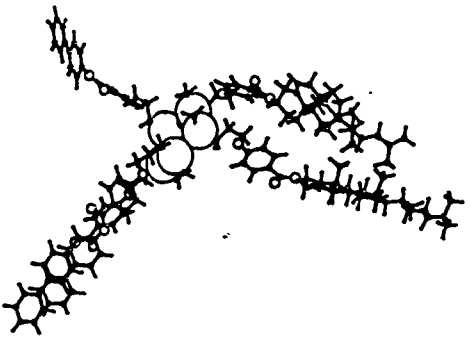

(a)

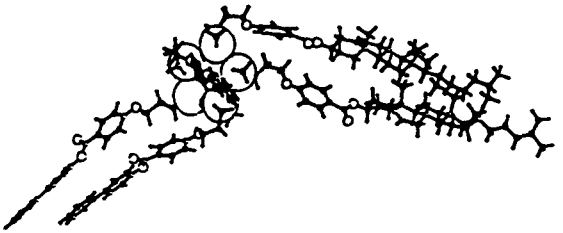

(b)

Figure 7: Model structures of the cylinder isomer after a 10 pico second molecular dynamics simulation. The upper structure (a) is the lowest energy conformation adopted during the simulation. The lower structure (b) is the statistically averaged structure of the molecule during the 10 pico second simulation.

the *Tor1* angles in the three models from the 10 pico second dynamics simulation. Table II mostly relates the initial model to the "equilibrated" structure, while Table III relates to deviations from this equilibrated structure during the MD run.

TABLE II : <*Tor1*>[a] and <*ΔTor1*>[b] Mean Dihedral Angles (°) from the Molecular Dynamics (MD) Simulation in Comparison to the Initial Values

Mesogen Type		Isolated Cone		Isolated Disk		Isolated Cylinder	
		<*Tor1*>	<*ΔTor1*>	<*Tor1*>	<*ΔTor1*>	<*Tor1*>	<*ΔTor1*>
{C}	Initial	60		63		185	
	MD	55	5	74	11	176	9
{C}	Initial	45		59		300	
	MD	68	23	54	5	283	17
{B}	Initial	180		54		60	
	MD	153	27	65	11	66	6
{B}	Initial	180		175		61	
	MD	284	104	195	20	64	3
{B}	Initial	40		55		69	
	MD	187	147	71	16	67	2

[a] *Tor1* = {O-Si-$C_{\text{first of spacer-mesogen}}$-$C_{\text{second of spacer-mesogen}}$}.

[b] The mean variation of the torsion as compared to the initial value.

TABLE III : Range of the *Tor1* Dihedral Angles (°) during the Molecular Dynamics (MD) Simulation

Mesogen Type	Isolated Cone	Isolated Disk	Isolated Cylinder
{C}	49	88	56
{C}	50	62	38
{B}	50	170	84
{B}	56	76	58
{B}	42	74	41

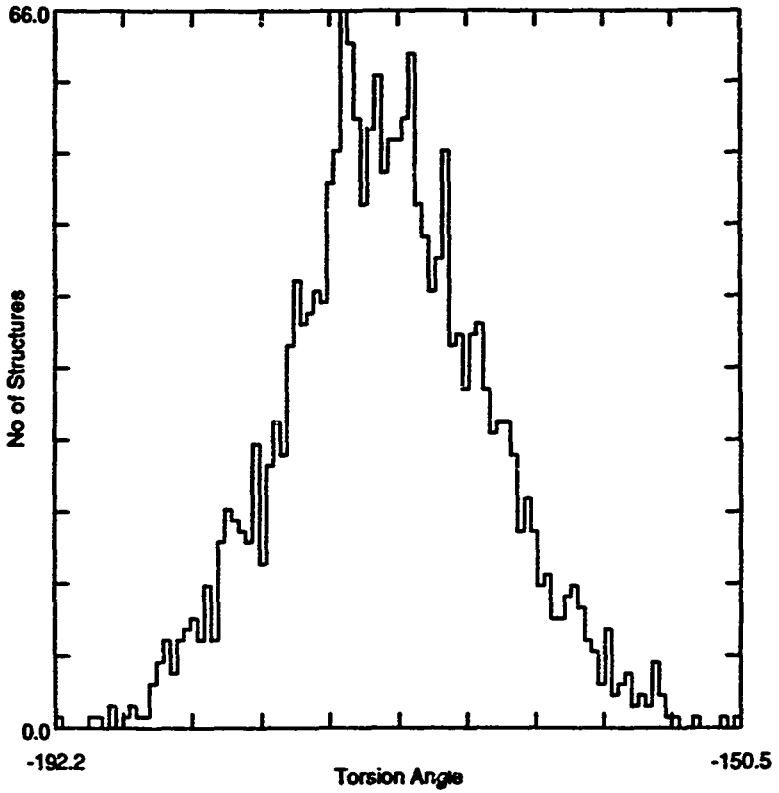

Figure 8: Statistical data of the 10 pico second molecular dynamics simulation : histogram of a *Tor1* dihedral angle variation during the 10 pico second molecular dynamics simulation for an isolated cone model.

Notably, the largest conformational flexibility around this bond is observed in the cone model, with two of the dihedral angles (on {**B**} mesogens) varying by 104°, and 147° on average from the initial magnitudes, while all other <*Tor1*> differences are smaller than 30°. The large variations of this dihedral angle may reflect, in part, the stability of a particular model with respect to the proximity of the mesogens. Thus, the result is anticipated since the cone model with all of the mesogens at an axial position is the least stable energetically (the minimum energies of the initial cone, disk, and cylinder models are 309, 298, and 260 kcal/mol, respectively)[16]. The average <Δ*Tor1*> values are 61°, 13°, and 7° for the cone, disk, and cylinder models, respectively. This relative flexibility of the cone model is also reflected in the range values shown in Table III. The values for the cone model are on average (= 49°) much smaller than those for the disk model (= 94°), indicating a lower conformational flexibility of the mesogens. This may be due to an increase in the steric interactions among the mesogens for the cone relative to the disk model. Interestingly, although the cylinder model has the lowest minimum energy of the three[16], its mesogens have on average a lower conformational flexibility than those in the disk, as also evidenced by a lower average range of torsion angles (= 55°).

A different pattern of variations in these models is observed for the *Tor2* torsions (defined by the position of the mesogen relative to the ring : {Si-O-Si-$C_{\text{first of spacer-mesogen}}$}) which describe possible flexibility in the orientation of the mesogens relative to the siloxane ring Statistical data of the results, tabulated for the cone, disk and cylinder models in Tables IV and V, indicate the largest conformational flexibility around this bond is observed for the cone model with all of the five dihedral angle differences in the range of ±120°. The average |<Δ*Tor2*>| values are 121°, 75°, and 71° for the cone, disk, and cylinder models, respectively. Specifically, two of the mesogens which had an initial *Tor2* torsion of -60° with respect to the siloxane ring assume mean values of ca. 180°, thus resembling the cylinder model. Once again, this may indicate a lower stability for the cone model. In general, however, all of the three models exhibit large changes in the mesogen's orientation relative to the siloxane ring. The range of torsion angles shown in Figures 9(a)-(c) indicate that both the cone and cylinder model ranges are approximately 60° for all

angles, while a larger range is observed for the disk model. These changes can be clearly seen in Figure 6. The greatest possibility for conformational flexibility in the position of the mesogens relative to the siloxane ring is exhibited by the disk model. This can be explained, in part, by lower steric interactions between mesogens in this case, enabling easy reorientation.

TABLE IV : <*Tor2*>[a] and <*ΔTor2*>[b] Mean Dihedral Angles (°) from the Molecular Dynamics (MD) Simulation in Comparison to the Initial Values

Mesogen Type		Isolated Cone		Isolated Disk		Isolated Cylinder	
		<*Tor2*>	<*ΔTor2*>	<*Tor2*>	<*ΔTor2*>	<*Tor2*>	<*ΔTor2*>
{C}	Initial	304		176		184	
	MD	184	120	295	119	189	5
{C}	Initial	306		176		309	
	MD	172	134	49	127	59	110[c]
{B}	Initial	303		194		298	
	MD	63	120[c]	183	11	169	129
{B}	Initial	305		176		293	
	MD	59	114[c]	176	0	282	11
{B}	Initial	299		54		175	
	MD	181	118	293	121[c]	77	98

[a] *Tor2*= {Si-O-Si-$C_{\text{first of spacer-mesogen}}$}.

[b] The mean variation of the torsion as compared to the initial value.

[c] The absolute value of the variation is given.

TABLE V : Range of the <*Tor2*> Dihedral Angles (°) during the Molecular Dynamics (MD) Simulation

Mesogen Type	Isolated Cone	Isolated Disk	Isolated Cylinder
{C}	69	86	36
{C}	62	90	68
{B}	60	78	117
{B}	66	169	67
{B}	49	90	96

The flexibility of the alkoxybenzoate group was defined as *Tor3* (C-C-O-{phenyl}). These dihedral angles (one/mesogen) describe the ability of the mesogens to rotate with respect to the

leader group. In order to be consistent with the proposed model of interdigitation[13,16], the mesogens would in some instances need to be splayed (kinked) with respect to the director in order to maintain continuous lamellar packing. A primary location for this kinking to take place may be at this ester bond. Tables VI and VII indicate that the disk model has the greatest range (= 64°, 125°, and 55° for the cone, disk, and cylinder models, respectively) and the lowest average difference in the mean dihedral angles (= 48°, 31°, and 42° for the cone, disk, and cylinder models, respectively). The average range for the disk model is almost twice that of the cone and cylinder models, which may foretell a greater tendency towards interdigitation for this model. It is interesting to point out that with the exception of the disk model (which has one gauche bond), all of the mean <*Tor3*> values derived from the dynamics simulation assume nearly a transorientation of approximately 180°.

Changes in the *Tor1*, *Tor2*, and *Tor3* torsional angles indicate that the disk model exhibits a larger conformational flexibility than the cylinder and cone models. Especially indicative are the large range, yet the relatively small difference between the initial and mean MD dihedral angles for the disk model. The advantage in flexibility for the disk may be important with regard to the LC phase behavior observed for these materials. In general, the amount of interdigitation is primarily governed by the flexibility of the leader groups and of the attached mesogens[28]. Also important is the persistence of the interdigitation, which may also be influenced by the conformational flexibility. Based on these two criteria, the data may support the disk model over the other two as a more favorable choice for a model of a highly interdigitated, splayed mesogenic LC phase.

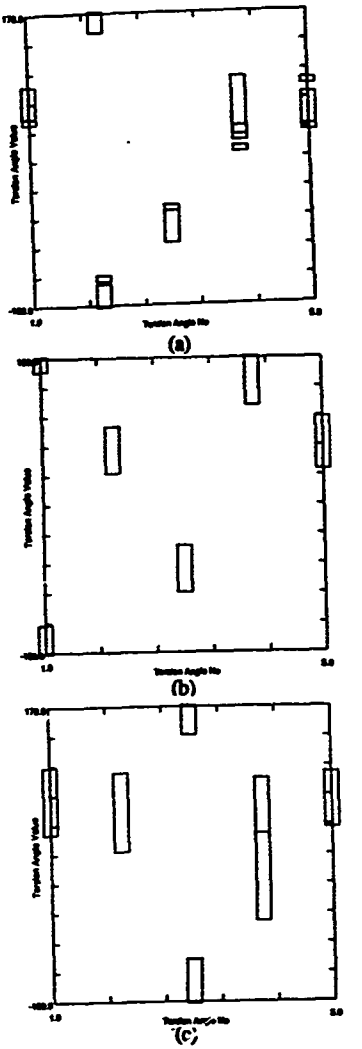

Figure 9: Statistical data of the 10 pico second molecular dynamics simulation : box range map displaying the variation in the torsion angles about the single bond connecting each sidechain to the siloxane ring (*Tor2*) : (a) - (c) correspond to the cone, disk, and cylinder isolated models, respectively.

TABLE VI : <*Tor3*>[a] and <Δ*Tor3*>[b] Mean Dihedral Angles (°) from the Molecular Dynamics (MD) Simulation in Comparison to the Initial Values

Mesogen Type		Isolated Cone		Isolated Disk		Isolated Cylinder	
		<*Tor3*>	<Δ*Tor3*>	<*Tor3*>	<Δ*Tor3*>	<*Tor3*>	<Δ*Tor3*>
{C}	Initial	177		177		179	
	MD	173	4	184	7	188	9
{C}	Initial	185		170		179	
	MD	148	37	185	15	177	2
{B}	Initial	119		183		76	
	MD	190	71	294	111	179	103
{B}	Initial	171		173		85	
	MD	202	31	161	12	169	84
{B}	Initial	91		175		183	
	MD	186	95	165	10	171	12

[a] *Tor3* = (C-C-O-{phenyl}).

[b] The mean variation of the torsion as compared to the initial value.

TABLE VII : Range of the <*Tor3*> Dihedral Angles (°) during the Molecular Dynamics (MD) Simulation

Mesogen Type	Isolated Cone	Isolated Disk	Isolated Cylinder
{C}	55	179	48
{C}	103	137	43
{B}	58	137	72
{B}	52	94	41
{B}	52	78	71

The rotatable bonds between the two phenyl rings in the three {B}mesogens (*Tor4*) as shown in Tables VIII and IX, were also examined. The results show little difference between the models. Figures 10(a)-10(c) depict the variations in one of the *Tor4* angles during the simulation, showing the behavior of the three models to be similar. Note that although the disk, cone, and cylinder structures have changed considerably during the molecular dynamics simulation, they are still termed as such in order to be able to distinguish between different starting models.

TABLE VIII : <*Tor4*>[a] and <*ΔTor4*>[b] Mean Dihedral Angles (°) from the Molecular Dynamics (MD) Simulation in Comparison to the Initial Values

Mesogen Type		Isolated Cone		Isolated Disk		Isolated Cylinder	
		<*Tor4*>	<*ΔTor4*>	<*Tor4*>	<*ΔTor4*>	<*Tor4*>	<*ΔTor4*>
{B}	Initial	0		0		-2	
	MD	9	9	6	6	6	8
{B}	Initial	0		0		10	
	MD	-6	6	-12	12	-2	12
{B}	Initial	0		0		-6	
	MD	-4	4	-9	9	-12	6

[a] Rotatable bond between the two phenyl rings in the three {B}mesogens.

[b] The mean variation of the torsion as compared to the initial value.

TABLE IX : Range of the <*Tor4*> Dihedral Angles (°) during the Molecular Dynamics (MD) Simulation

Mesogen Type	Isolated Cone	Isolated Disk	Isolated Cylinder
{B}	46	43	35
{B}	78	88	72
{B}	87	91	73

The final set of dihedral angles examined were those within the siloxane ring (*Tor5* = {Si-O-Si-O(1) and O-Si-O-Si(2)}). Tables X and XI indicate the large amount of flexibility and conformational variation present in the siloxane ring. Once again, the disk model exhibits the greatest flexibility, further supporting the assumption that the disk may be the most favorable conformation in a LC phase.

TABLE X : <*Tor5*>[a] and <*ΔTor5*>[b] Mean Dihedral Angles (°) from the Molecular Dynamics (MD) Simulation in Comparison to the Initial Values

Type		Isolated Cone		Isolated Disk		Isolated Cylinder	
		Value	Difference	Value	Difference	Value	Difference
1	Initial	60		290		187	
	MD	182	122	292	2	287	100
2	Initial	59		76		177	
	MD	183	124	54	22	52	125
1	Initial	299		299		285	
	MD	66	127[c]	64	125[c]	181	104
2	Initial	299		59		64	
	MD	292	7	297	122[c]	175	111
1	Initial	300		293		58	
	MD	70	130[c]	182	111	57	1
2	Initial	60		66		297	
	MD	304	116[c]	184	118	310	13
1	Initial	297		297		208	
	MD	173	124	315	18	178	30
2	Initial	64		59		173	
	MD	176	112	61	2	170	3
1	Inital	300		68		298	
	MD	64	124[c]	179	111	276	22
2	Initial	161		295		56	
	MD	302	41	173	122	143	87

[a] Siloxane ring torsions : {Si-O-Si-O$^{Type\ 1}$ and O-Si-O-Si$^{Type\ 2}$.

[b] The mean variation of the torsion as compared to the initial value.

[c] The absolute value of the variation is given.

TABLE XI : Range of the <*Tor5*> Dihedral Angles (°) during the Molecular Dynamics (MD) Simulation

Isolated Cone	Isolated Disk	Isolated Cylinder
53	69	84
56	79	111
58	68	73
62	84	64
63	113	43
64	78	39
69	60	76
65	59	72
49	77	91
47	89	94

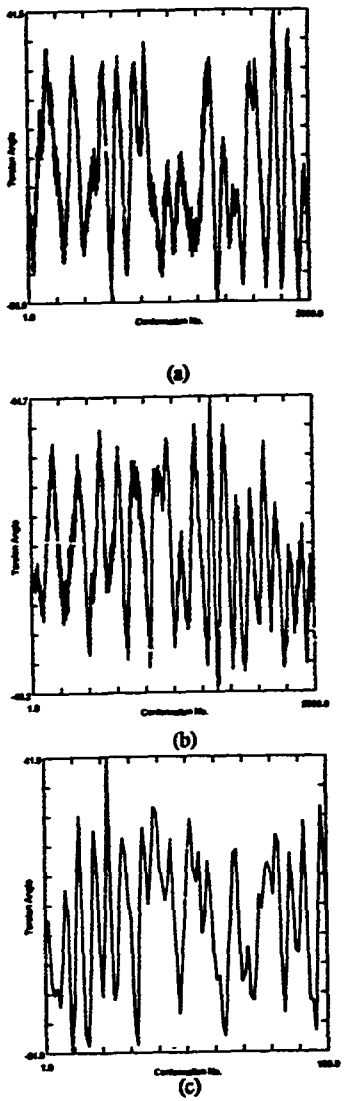

Figure 10: Statistical data of the 10 pico second molecular dynamics simulation : trace of the variation in a dihedral angle *Tor3* : (a) - (c) correspond to the cone, disk, and cylinder isolated models, respectively.

3.2. Dynamics on Molecular Pairs

Molecular dynamics simulations were also carried out on molecular pairs. Intermolecular ordering patterns considered for the global molecular topologies were based on the "interdigitation of mesogens" structural supposition based on experimental data[13]. In particular, the cylinder and the disk models were examined at this stage, since the cone model was shown to be less stable than the disk and cylinder.

3.2.1 Cylinder Model

Previous X-ray diffraction measurements made on these cyclic siloxane-based LC's indicate a primary d-spacing of ~ 25 Å[13]. This distance apparently corresponds to the partial interdigitation of the {B} and {C} mesogens of the proposed cylinder model (cf. Figure 11). These molecules mark the starting point of the molecular dynamics simulation. Results of such a simulation may indicate to what degree the {B} and {C} mesogens remain interdigitated, if at all. Two different simulations were performed, discussed in detail below.

3.2.1.1 CASE I - Unconstrained Molecules

The starting structure for this simulation is the model shown in Figure 11. Two cylinder molecules, each minimized to remove large distortions in geometry and bad steric interactions, were moved next to one another and their *inter*molecular energies were minimized. Less than five van der Waals close contacts (between 2.6 Å and 3.0 Å) were found in the final interdigitated structure. A molecular dynamics simulation (details are presented in Table Ib) was performed, with the resulting lowest energy and statistically averaged structures from the dynamics run shown in Figure 12. Because no constraints were placed on the siloxane rings in these molecules, they do not remain parallel to one another. This freedom of rotation might not be as energetically

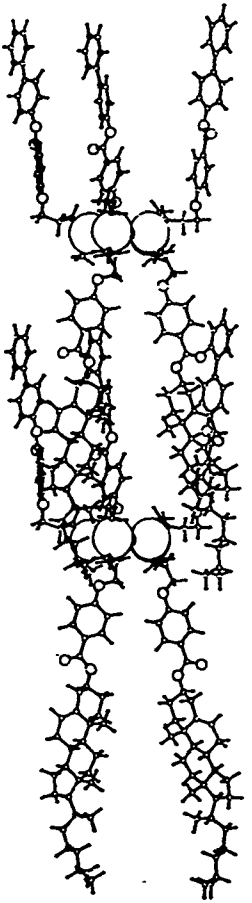

(c)

Figure 11: Optimized geometry of the cylinder interdigitated pair model used in molecular dynamics calculations.

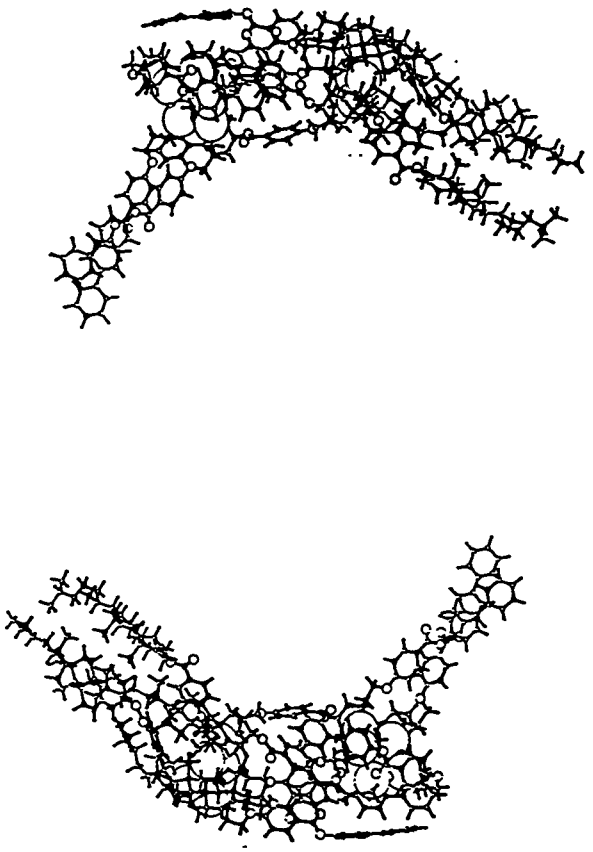

Figure 12: Model structure of the unconstrained cylinder interdigitated pairs (CASE I) after a 10 pico second molecular dynamics simulation. The upper structure is the lowest energy relationship adopted by the molecules during the simulation. The lower structure is the statistically averaged structure of the molecule pairs during the simulation.

favorable in the LC phase due to constraints from other nearby molecules in the system. This will be dealt with by constraining the siloxane rings (CASE II of this section). Nonetheless, it is most interesting to note the large degree of interdigitation among the biphenyl and cholesteryl mesogens. The extent of the interdigitation in this structure (after a 10 pico second dynamics simulation) is comparable to that seen in the minimum energy starting structure. This result lends support to the model which was proposed by Bunning et. al.[13], suggesting that the pendant mesogens may indeed be interdigitated in the LC phase, thus accounting for the primary d-spacing observed with X-ray diffraction studies. Although a short simulation time was used, the total dynamics run (including equilibration) was 140 ps, showing no tendency of the system to dissociate.

Statistical data for the interior mesogens torsion angles was also examined. In general, it is shown that the torsional angle *Tor1* (Table XII) varies in a range of 30° to 60° for the interior mesogens of this twin cylinder model. Figures 13(a) and 13(b) depict an example of the variation in one of the *Tor1* angles during the simulation (respectively for each one of the interdigitated molecules). Surprisingly, there is not a remarkable difference in the conformational flexibility or stability of the interdigitated mesogens when compared to the results for an isolated cylinder. In both cases, the differences in the dihedral angles are small and the range similar, except for one of the torsions which changes from an initial value of 69° to a mean value of 181° during the simulation. The average range for the interdigitated mesogens is slightly lower due to possible interactions introduced upon packing.

The statistical data for *Tor3* shown in Table XIII reveals little difference for this dihedral angle between interdigitated structure and that of the isolated cylinder, and only two of the angles are changing markedly during the simulation. In both cases there is a tendency of these angles to assume values of ca. 180°.

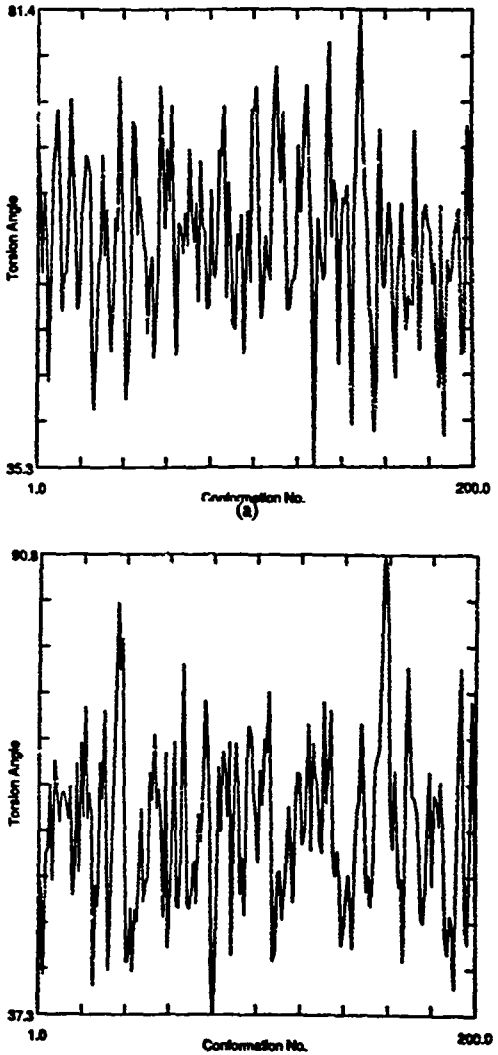

Figure 13: Statistical data of the 10 *pico* second molecular dynamics simulation : trace of the variation in a dihedral angle *Tor1* : (a) and (b) correspond to the two interdigitated cylinders.

Table XII: Mean Dihedral Angles and Range of Variations for the <*Tor1*>[a] Torsion for the Unconstrained Cylinder Model

					Isolated Cylinder	
Mesogen Type	**Initial**	**Mean of Dynamics**	**Difference**	**Range**	**Difference**	**Range**
{C}	185	177	8	39	9	41
{C}	300	292	8	36	17	56
{B}	69	181	112	40	6	38
{B}	61	55	6	46	3	84
{B}	60	56	4	59	2	58

[a] See footnote a of Table II.

Table XIII: Mean Dihedral Angles and Range for the <*Tor3*>[a] Torsion for the Unconstrained Cylinder Model

					Isolated Cylinder	
Mesogen Type	**Initial**	**Mean of Dynamics**	**Difference**	**Range**	**Difference**	**Range**
{C}	179	193	14	344	116	41
{C}	179	181	2	43	12	71
{B}	85	197	112	70	103	72
{B}	183	187	4	55	9	48
{B}	76	258	182	36	2	43

[a] See footnote a of Table VI.

The range during the MD simulation for *Tor4* and *Tor2* is shown in Figures 14(a) and 14(b) for the left molecule, and similarly in Figures 15(a) and 15(b) for the right molecule of the interdigitated system. Interestingly, the ranges of change in *Tor2* are relatively small in both molecules (Figures 14(b) and 15(b)), showing no large change in the amount of interdigitation These ranges are again very similar to those exhibited by the isolated cylinder model.

On the other hand, larger changes are observed in *Tor5* for the cylinder pair than for the isolated cylinder model This is apparent when comparing the <*ΔTor5*> for example for the eight first angles shown in Table XIV to the corresponding values shown in Table X and XI, with the

average magnitudes being larger by 35° and 18° for the left and right siloxane rings, respectively. The average range is larger by 27° for the right siloxane ring than that for the isolated cylinder case. This indicates that the siloxane ring undergoes a large amount of torsional changes during the simulation when the mesogens are interdigitated.

Table XIV: Mean Dihedral Angles and Range of Variations for the <*Tor5*>[a] Torsions for the Unconstrained Cylinder Model

Initial	Dynamics Left	Mean Difference Left	Dynamics Right	Mean Difference Right	Range Left	Range Right
187	181	6	176	11	61	59
177	181	16	193	16	67	61
285	335	50	325	40	92	133
64	317	253	346	282	78	127
58	147	89	147	89	109	97
297	279	18	291	6	88	60
208	281	73	261	53	52	148
173	59	114	45	128	46	130

[a] See footnote a of Table X.

3.2.1.2 CASE II - Constrained Molecules

The starting structure of the model used in this simulation is identical to the starting structure used in CASE I except for the presence of atom constraints. To eliminate the ability of the siloxane rings to change their relative orientation, atom constraints were applied to all atoms making up the siloxane rings. These constraints forced the selected atoms to remain fixed at their initial minimized {x,y,z} coordinates. Thus, by constraining the rings it was expected that the effects of an LC phase would be better modeled. The details of the molecular dynamics calculation are presented in Table Ic.

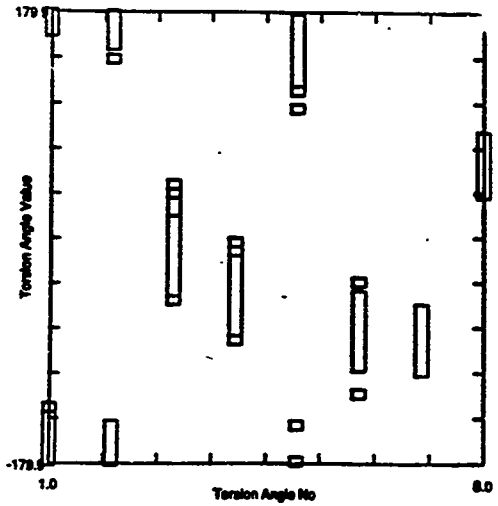

(a)

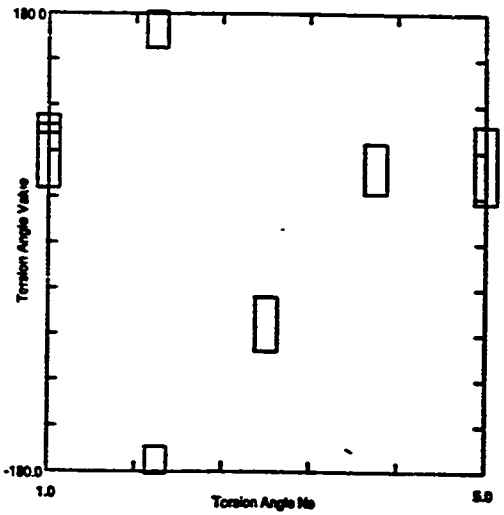

(b)

Figure 14: Statistical data for the left molecule in the unconstrained cylinder pair model after a 10 pico second dynamics simulation. (a) a box range map displaying the variation in torsion angle (*Tor4*) about the single bond connecting each sidechain to the left siloxane ring. (b) a box range map displaying the variation in torsion angles *Tor2* in the left siloxane ring.

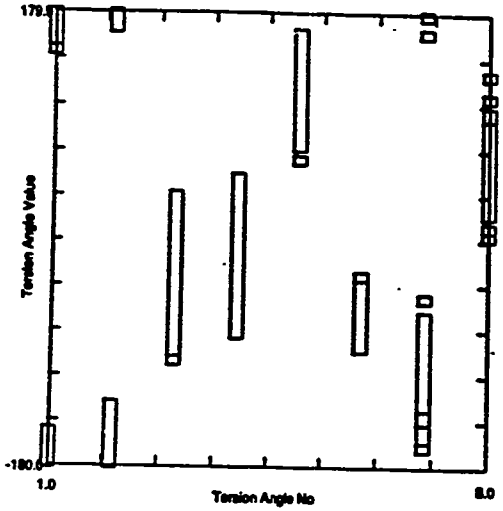

(a)

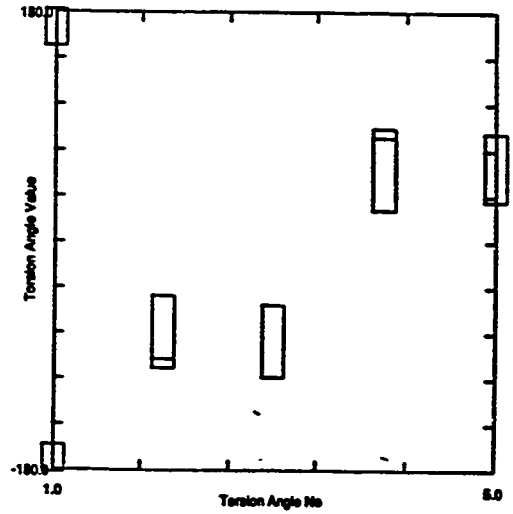

(b)

Figure 15: Statistical data for the right molecule in the unconstrained cylinder pair model after a 10 pico second dynamics simulation. (a) a box range map displaying the variation in torsion angle (*Tor4*) about the single bond connecting each sidechain to the right siloxane ring. (b) a box range map displaying the variation in torsion angles *Tor2* in the right siloxane ring.

The low energy and the statistically averaged structures are shown in Figure 16. In each case the degree of interdigitation is less than in CASE I, as the pendant mesogens, especially {B}, move outward from the central region between the siloxane rings. Because the degree of interdigitation in CASE II is less than in CASE I, another dynamics simulation is to be performed in which two interdigitated molecules are surrounded by additional molecules in order to create boundary conditions for the inner two molecules which would better describe the LC state.

An examination of the changes in the torsions during the simulation reveal differences between CASE I and CASE II of the dynamics simulation. Table XV shows the statistical data from the interior mesogens for the constrained cylinder model. The average range of flexibility for this model of ca. 90° is much larger than either the isolated or unconstrained cylinder models This model also has a larger average difference between initial and mean dihedral angles (= 61°). Figures 17(a) and 17(b) depict the variation in one of the *Tor1* angles during the simulation (for each one of the interdigitated molecules) in which a large change was observed, clearly seen also in Figure 16. By constraining the siloxane ring, larger torsional movements of the leader group near the siloxane ring (*Tor1*) were observed, while the range and average difference for the *Tor3* torsions were very similar to those of the unconstrained case because it was several atoms away. Contrary to this behavior, the *Tor2* values did not change as much as in the unconstrained case because of the hinderance to ring movement. The *Tor4* and *Tor5* values are very similar to the unconstrained and isolated cylinder model values due to the siloxane rings being hindered.

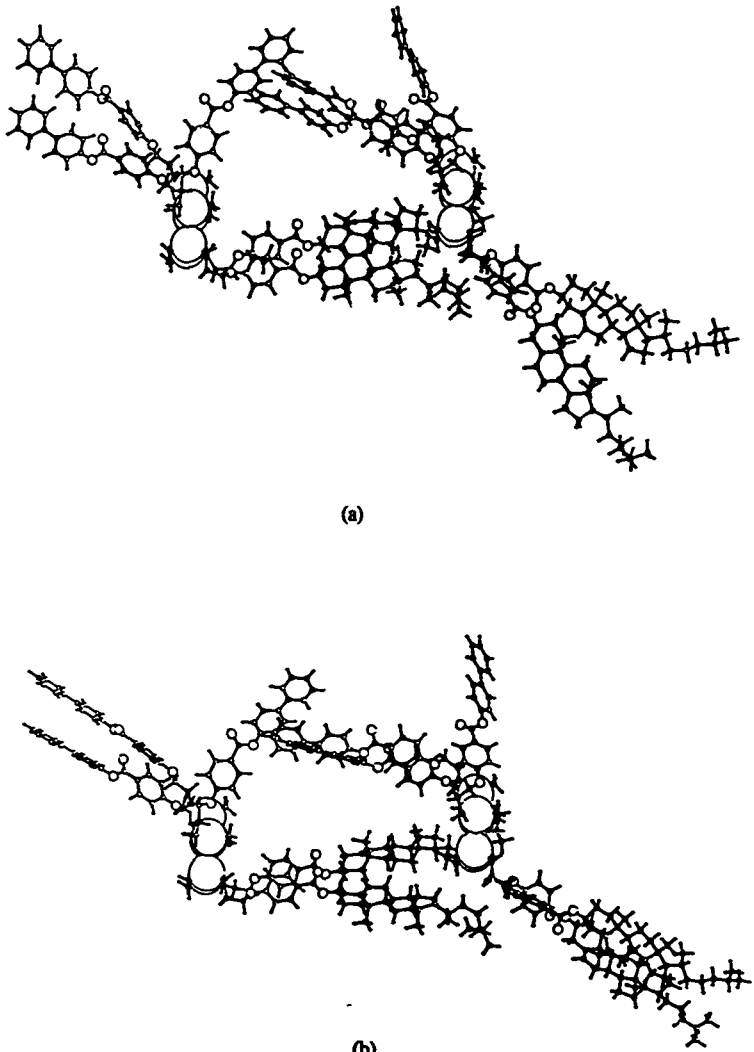

Figure 16: Model structure of the constrained cylinder interdigitated pairs (CASE II) after a 10 pico second MD simulation. The upper structure is the lowest energy relationship adopted by the molecules during the simulation. The lower structure is the statistically averaged structure of the molecule pairs during the simulation.

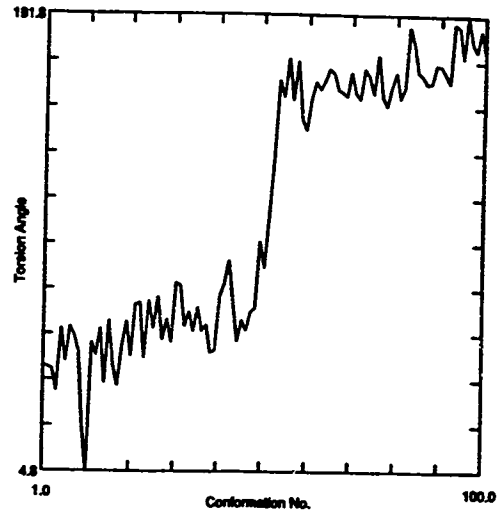

(a)

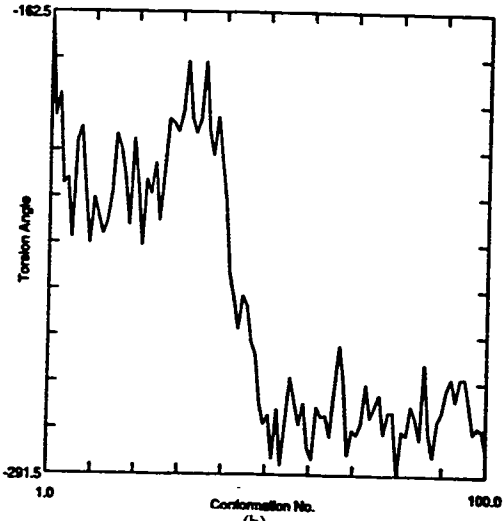

(b)

Figure 17: Statistical data of the 10 pico second molecular dynamics simulation : trace of the variation in a dihedral angle *Tor1* : (a) and (b) correspond to the two interdigitated cylinders. These angles correspond to those shown in Figure 13.

Table XV: Mean Dihedral Angles and Range of Variations for the <*Tor1*>[a] Torsion for the Constrained Cylinder Model

					Isolated Cylinder	
Mesogen Type	Initial	Mean Dynamics	Difference	Range	Difference	Range
{C}	185	82	103	129	9	41
{C}	300	300	0	39	17	56
{B}	69	79	10	38	6	38
{B}	61	115	54	187	3	84
{B}	60	200	140	44	2	58

[a] See footnote a of Table II.

3.2.2 Disk Model

3.2.2.1 CASE III - Constrained Molecules

As in the cylinder model, in which partial interdigitation of the mesogens corresponds to the primary d-spacing observed in X-ray diffraction studies, the partial interdigitation of these mesogens in the disk model may also correspond to the observed X-ray data. Molecular dynamics calculations were performed on two interdigitated disk molecules, each minimized to its minimum energy conformation as seen in Figure 18. As was done before, the *inter*molecular energy between the two molecules was minimized and less than five van der Waals close contacts were found in the final structure. Atom constraints were also imposed in this simulation in order to maintain the initial relationship between the two siloxane rings. All atoms in the siloxane rings were constrained to their initial minimized {x,y,z} coordinates. The details of this simulation are given in Table Id. The low energy and the statistically averaged structure of this system after a 10 pico second simulation are shown in Figure 19.

The range during the molecular dynamics simulation for *Tor2* and *Tor5* is very small since the rings are constrained. Statistical data for the *Tor1* torsions show relatively large variations

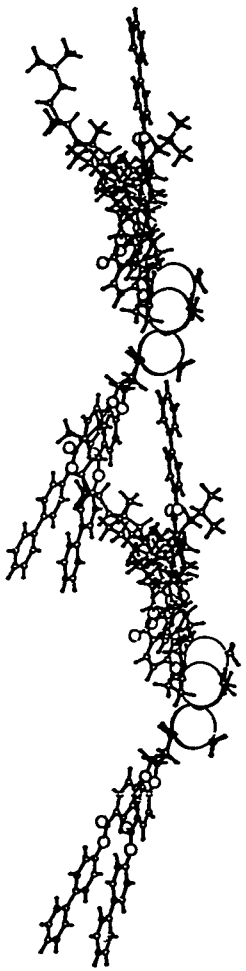

Figure 18: Optimized geometry of the disk interdigitated pair model used in molecular dynamics calculations.

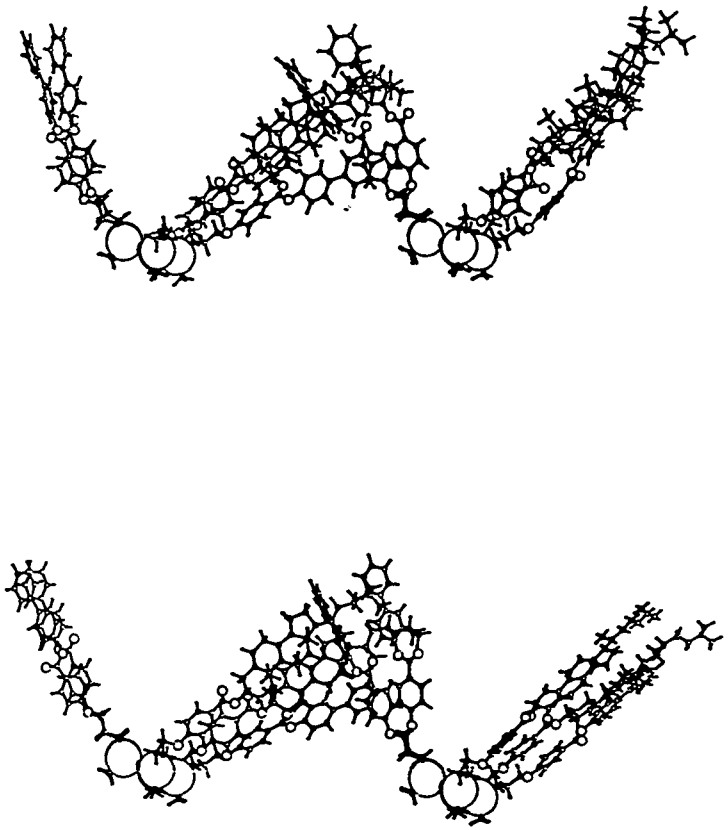

Figure 19: Model structure of the constrained disk interdigitated pairs (CASE III) after a 10 pico second molecular dynamics simulation. The upper structure is the lowest energy relationship adopted by the molecules during the simulation. The lower structure is the statistically averaged structure of the molecule pairs during the simulation.

analogous to the constrained cylinder model. Indeed, it is interesting to note that the so called disk model transforms into a conformation more resembling the cone model of Figure 2. A more extensive dynamics simulation, similar to the one mentioned in the previous section should be conducted here in order to provide additional boundary conditions to the molecules. Also, a pair of unconstrained disk models should be studied in order to examine if the siloxane rings absorb energy in a manner analogous to the unconstrained cylinder model. Finally, it should be noted that the disk model proposed[16] is somewhat different than the disk model examined here. The proposed model has a unit director associated with it as the mesogens have been splayed so that they point in one direction. The disk system examined here is more analogous to a radial system with the mesogens radiating in all directions

3.3. X-ray Diffraction Simulations

Simulated X-ray diffraction patterns of the two cylinder pair systems (CASES I and II) and of the disk pair system (CASE III) were examined. The simulated meridional scattering patterns for the unconstrained cylinder model (CASE I) are shown in Figures 20(a)-20(d). Additional reflections appear for the final structure as compared to the initial structure. The origin of the large peak in these scans at $2\theta=1.405^{o}$, d=62.8Å may be due to the relatively small numbers of units interdigitated. It has been shown that longer units have an effect on the resulting X-ray pattern[16] due to effects of the noninterdigitated end mesogens. Scattering patterns for the constrained cylinder model (CASE II) are shown in Figures 21(a)-21(d). Once again, there is considerable change in the scattering pattern between the first and last structure of the dynamics simulation. Table XVI summarizes the d-spacings of these structures for CASES I and II. Clearly, an increase in the number of peaks in the meridional scans indicates that CASE II is a more ordered structure. The equatorial scattering patterns for the disk pair model (CASE III) are shown in Figure 22.

Table XVI: X-ray Diffraction Maxima (Å) from Calculated Meridional Scattering Patterns of the First and Last Structures (CASES I & II)

CASE I		CASE II		Experimental[13]
First	Last	First	Last	
62.8	62.8	62.8	62.8	
15.7	20.9	20.9	20.9	24.0
	10.4	12.6	12.6	11.9
	7.0	7.9	7.9	8.0
		5.7	6.3	6.0
			4.8	

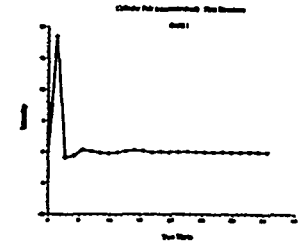

(a)

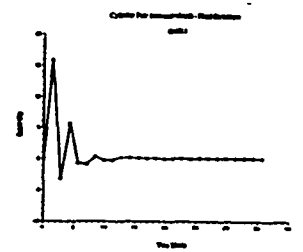

(b)

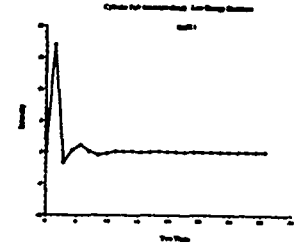

(c)

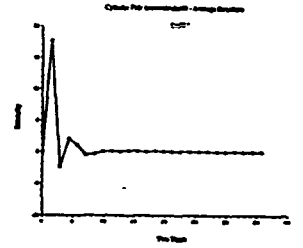

(d)

Figure 20: CASE I: Meridional scattering section for (a) the starting structure of the 10 pico second MD simulation. (b) the final structure of the 10 pico second simulation. (c) the lowest energy structure of the 10 pico second simulation. (d) the statistically averaged structure of the 10 pico second simulation. Incident X-ray beam is perpendicular to the siloxane rings.

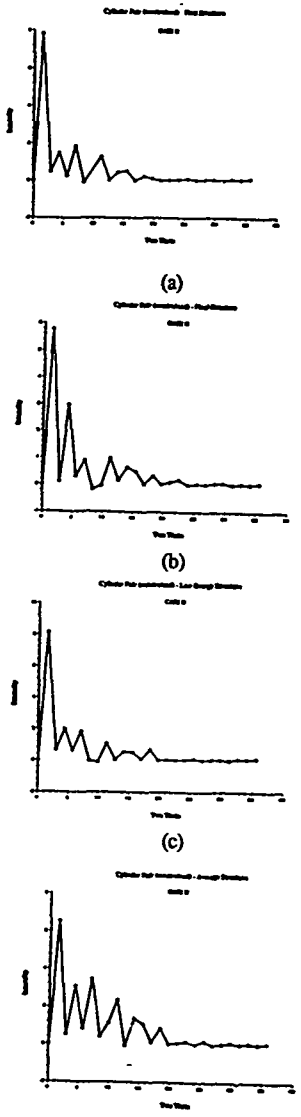

(a)

(b)

(c)

(d)

Figure 21: CASE II: Meridional scattering section for (a) the starting structure of the 10 pico second MD simulation. (b) the final structure of the 10 pico second simulation. (c) the lowest energy structure of the ten ps simulation. (d) the statistically averaged structure of the 10 pico second simulation. Incident X-ray beam is perpendicular to the siloxane rings.

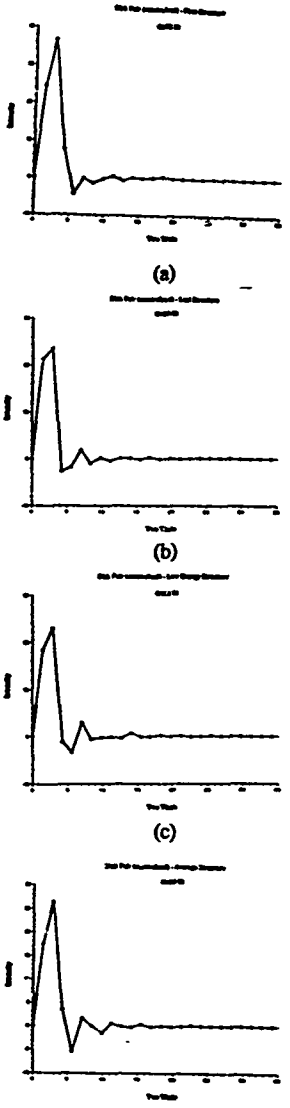

Figure 22: CASE III : Equatorial scattering section for (a) the starting structure of the 10 pico second MD simulation. (b) the final structure of the 10 pico second simulation. (c) the lowest energy structure of the t10 pico second simulation. (d) the statistically averaged structure of the 10 pico second simulation. Incident X-ray beam is perpend to the siloxane rings.

Section 4

CONCLUSIONS

Molecular dynamics simulations offer new insights into the conformational flexibility of these cyclic siloxane-based LC's. Interdigitation between the cholesteryl 4' - allyloxybenzoate and biphenyl 4' - allyloxybenzoate mesogens pendant on the siloxane ring is certainly present in the simulated structure, but a quantitative measure of the interdigitation is still to be calculated, possibly by the application of boundary conditions to the system. The isolated disk model exhibited the most flexibility and greatest stability as indicated by mean dihedral angles and range for certain key torsions. In general, all three isolated models displayed large conformational flexibility, which may be important with regard to the LC phase behavior. Results from the dynamics simulation of the cylinder pairs indicate the large conformational flexibility of the siloxane rings. Movements of the interdigitated mesogens were much higher for a fixed rings system than for the case where the ring dihedral angles were free to move. X-ray scattering pattern calculations for the structures generated during the dynamics run demonstrate higher order than for the initial models, as shown in Table XVI.

REFERENCES

(1) Eich, M.; Wendorff, J. H.; Reck, B.; Ringsdorf, H. *Makromol. Chem., Rapid Commun.* **1987**, *8*, 59.

(2) Meredith, G. R.; Van Dusen, J. G.; Williams, D. J. *Macromolecules* **1982**, *15*, 1385.

(3) Sohn, J. E.; Singer, R. D.; Lalama, S. J.; Kuzyk, M. G. *Polym. Mat. Sci. Eng.* **1986**, *55*, 532.

(4) Gemmel, P. A.; Gray, G. W.; Lacey, D. *Polym. Prepr. Am. Chem. Soc. Div. Polym. Chem.* **1983**, *24*, 253.

(5) Tsai, M. L.; Chen, S. H.; Jacobs, S. D. *Appl. Phys. Lett.* **1989**, *54*, 2395.

(6) Ortler, R. ; Brauchle, C.; Miller, A.; Riepl, G. *Makromol. Chem., Rapid Commun.* **1989**, *10*, 189.

(7) Pinsl, J.; Brauchle, Chr.; Kreuzer, F. H. *J. Mol. Elec.* **1987**, *3*, 9.

(8) Davidson, P.; Levelut, A. M.; Achard, M. F.; Hardovin *Liquid Crystals* **1989**, *4*, 561.

(9) Diele, S.; Oelsner, S.; Kushel, F.; Hisgen, B.; Ringsdorf, H. *Mol. Crys. Liquid Crystals* **1988**, *155*, 399.

(10) Percec, V.; Hahn, B.; Ebert, M.; Wendorff, J. H. *Macromolecules* **1990**, *23*, 2095.

(11) Richards, R. D. C.; Hawthorne, W. D.; Hill, J. S.; White, M. S.; Lacey, D.; Semlyen, J. A.; Gray, G. W.; Kendrick, T. C. *J. Chem. Soc. Chem. Commun.* **1990**, *95*.

(12) Provided by F. H. Kreuzer of the Consortium fur Electrochemische Industrie of Germany.

(13) Bunning, T. J.; Klei, H. E.; Samulski, E. T.; Crane, R. L.; Linville, R. J. *Liquid Crystals* **1991**, in press.

(14) *Computer Simulation of Polymers*, Roe, R. J., 1991.

(15) (a) Sorensen, R. A., Liau, W. B., Boyd, R. H., *Macromolecules* **1988**, 21, 194.
(b) Rutledge, G. C., Suter, U. W., *Macromolecules* **1991**, 24, 1921.

(16) Pachter, R., Bunning, T.J.;Adams, W.W. *J. Comp. Polymer. Sci.* **1991**.

(17) "Quanta/CHARMm": release 3.0, Polygen Corporation, **1990**.

(18) Brooks, B.R., Bruccoleri, R.E., Olafson, B.D., States, D.J., Swaminathan, S., Karplus, M. *J. Comp. Chem.* **1983**, 4, 187.

(19) Grigoras, S., Lane, T.H., *J. Comp. Chem.* **1988**, 9, 25.

(20) *Dynamics of Proteins and Nucleic Acids*, McCammon, J. A., Harvey, S C., 1989.

(21) *The Peptides - Analysis, Synthesis, Biology* , Udenfriend, S., Meienhofer, J., 1985.

(22) Verlet, L., *Phys. Rev.* **1967**, 159, 98.

(23) Anderson, H. C., *J. Chem. Phys.* **1980**, 72, 2384.

(24) Ryckaert, J. P., Circotti, G., Berrenden, H. J. C., *J. Comp. Phys.* **1977**, 23, 327.

(25) van Gunsteren, W. F., Berendson, H. J. C., *Mol. Phys.* **1977**, 34, 1311.

(26) *Diffraction of X-Rays by Chain Molecules*; Vainsthein, B. K., Elsevier, 1966.

(27) "CERIUS" program and manual : release 2.1, Cambridge Molecular Design Corporation, **1990**.

(28) *Thermotropic Liquid Crystals* ; Gray, G. W., John Wiley, 1987.

U.S. Government Printing Office 648-127